Surface effects on the magnetic properties of ultrafine cobalt particles

M. Respaud, J. M. Broto, H. Rakoto, and A. R. Fert
Laboratoire de Physique de la Matiére Condensée, Insa-Complexe Scientifique de Rangueil, 31077 Toulouse Cedex, France and Service National des Champs Magnétiques Pulsés, Insa-Complexe Scientifique de Rangueil, 31077 Toulouse Cedex, France

L. Thomas and B. Barbara
Laboratoire Louis Néel, 25 avenue des Martyrs, 38042 Grenoble Cedex, France

M. Verelst, E. Snoeck, P. Lecante, and A. Mosset
C.E.M.E.S., C.N.R.S., 29 rue Jeanne Marvig, 31055 Toulouse Cedex, France

J. Osuna, T. Ould Ely, C. Amiens, and B. Chaudret
Laboratoire de Chimie de Coordination, 205 route de Narbonne, 31077 Toulouse Cedex, France
(Received 8 July 1997; revised manuscript received 14 October 1997)

Monodispersed nanoparticles of cobalt have been prepared by an original method using the decomposition under hydrogen of an organometallic precursor in the presence of a stabilizing polymer. Two colloids (Coll-I and Coll-II) have been obtained by changing the organometallic concentration in the polymer. Observation by high-resolution transmission electronic microscopy (HRTEM) showed Co particles well isolated and regularly dispersed in the polymer with a very narrow size distribution centered around 1.5 nm (Coll-I) and 2 nm (Coll-II) diameter. These particles are superparamagnetic above the blocking temperature 9 K (Coll-I) and 13.5 K (Coll-II). The particle size deduced from the analyses of the magnetic susceptibilities and magnetization curves are consistent with those measured by HRTEM. Magnetization at 5 K seems to saturate in fields up to 5 T leading to an enhanced mean magnetic moment per atom for both samples, where $\langle \mu_{\mathrm{Co}} \rangle = 1.94 \pm 0.05\ \mu_B$ for the smallest particles. High-field magnetization measurements, up to 35 T, increases nearly linearly with the applied field. This is equivalent to an increase of the mean magnetic moment with $\langle \mu_{\mathrm{Co}} \rangle = 2.1 \pm 0.1\ \mu_B$ at 35 T for the smallest particles. The effective magnetic anisotropies are found to be larger than that of the bulk materials and decrease with increasing particle size. This set of data allows us to conclude that the enhanced magnetization, its increase with applied magnetic field, and the enhanced effective magnetic anisotropy are associated with the large influence of the surface atoms and are more significant with decreasing size.
[S0163-1829(98)05005-X]

I. INTRODUCTION

The physical properties of nanoscale metal particles are presently the object of intensive research.[1] These species, at the border between the solid and molecular state, display novel properties resulting from surface or quantum size effects.[1,2] For example several measurements on free clusters evidence enhanced magnetic moment per atom for clusters of the $3d$ metal,[3,4] or the appearance of ferromagnetism for ultrasmall clusters of $4d$ metals.[5] Even if these results are consistent with theoretical calculations,[6,7] further characterizations of the particles will be needed in order to understand completely these phenomena. These characterizations are particularly necessary for studies on crystalline structure, magnetization processes, magnetic anisotropy, Curie temperature, superparamagnetism, quantum relaxation of the magnetization, etc. changes with cluster size. These studies can only be carried out on well isolated and supported particles with magnetic properties closed to those obtained for free clusters.

Several methods have been used to synthesize metal nanoclusters that include evaporation of metal atoms, microemulsion in an inert atmosphere, sonification, reduction of $CoCl_2$, reduction in inverse micelles, electrochemical generation in the presence of surfactants and nanostructured thin films obtained by low-energy cluster beam deposition.[8,9] Crystalline polynuclear coodination complexes[10,11] are ideal, since in this case exactly identical clusters are positioned periodically in a lattice. For instance, a monocrystal of a Mn_{12} compound allowed the unambiguous identification of the macroscopic quantum relaxation of the magnetization phenomena.[12] Unfortunately, well-defined coordination clusters have less than a few tens of atoms. Furthermore, the ligand shell will induce a perturbation of their magnetic properties.[10]

In order to investigate the possibility of obtaining small nanoclusters with a very narrow size distribution and without chemical bonding at the surface, we looked for an organometallic approach to the synthesis of metal nanoclusters. Thus, we have recently demonstrated that the decomposition of organometallic precursors in the presence of a reactive gas (H_2 or CO) could reproducibly lead to nonagglomerated metal particles displaying in some cases very narrow size distributions.[13,14]

The present work describes the properties of nanoscale metallic cobalt particle synthesized by the decomposition of the new organometallic precursor $Co(\eta^3\text{-}C_8H_{13})(\eta^4\text{-}C_8H_{12})$ (Ref. 15) in the presence of a stabilizing polymer. A prelimi-

nary account of the synthesis and properties of some of these clusters has been published.[14] Their size, morphology, and crystalline structure have been explored by high-resolution trasmission electron microscopy (HRTEM), wide angle x-ray scattering (WAXS), and magnetic measurements. Thus, we show the size modification of the size of the particles, which contains ca. 150 and 310 atoms, as a function of initial concentrations. Magnetic measurements evidence enhanced effective magnetic anisotropy and enhanced magnetization, compared to bulk values, and the absence of saturation in the magnetization even at 35 T, these features depending on cluster size. These results will be discussed in terms of the high surface-volume ratio, which has an influence on the magnetic moment per Co atom, on the effective magnetic anisotropy and on the magnetization process.

II. EXPERIMENTAL METHODS

The cobalt particles have been synthesized by the decomposition of the organometallic precursor $Co(\eta^3\text{-}C_8H_{13})(\eta^4\text{-}C_8H_{12})$ (Ref. 15) in the presence of a stabilizing polymer.[14] The reaction of a THF (TetraHydroFurane) solution of $Co(\eta^3\text{-}C_8H_{13})(\eta^4\text{-}C_8H_{12})$ (Ref. 15) with dihydrogen was carried out at 60 °C in a Fisher-Porter bottle in the presence of polyvinylpyrrolidone (PVP) for two different initial conditions, 10 wt % Co towards PVP (Coll-I), and 20 wt % Co (Coll-II). The solution was maintained under dihydrogen for 10 h in order to ensure complete reduction of the cobalt precursor. At this stage, the product deposited as a black material that was recovered by filtration, and could be dissolved again in THF or CH_2Cl_2 for further use. Finally, we obtained two different colloids with 11 w % Co for Coll-I and 12.81 w % Co for Coll-II diluted in the polymer.

Further charaterization of the different colloids was achieved by reacting them with CO (respectively, Coll-I′, Coll-II′) at room temperature in dichloromethane. An infrared spectrum of the resulting solution shows two absorptions at ca. 2000 and 1890 cm^{-1}, in agreement with the presence of terminal and doubly bridging CO groups at the surface of the particles and similar to previous results obtained for CO adsorbed on cobalt surfaces in ultravacuum conditions.[16] No sharp absorptions attributable to small molecular complexes or clusters and no high-frequency CO stretching modes resulting from the presence of partially oxidized cobalt surfaces were observed.

The size distribution and the morphology of the Co particles were studied by HRTEM performed on a Philips CM30/ST operating at 300 kV whose point resolution is 1.9 Å. Crystalline structure was studied by both HRTEM and WAXS. In order to avoid any possible oxidation of the cobalt particles, the samples were prepared in a glove box under an argon atmosphere. For HRTEM experiments, the powder was dissolved in THF and the resulting solution was deposited onto a copper grid covered by a thin carbon film.

For WAXS experiments, several samples were prepared by carefully sealing Co PVP powder in Lindemann capillaries (diameter$=1.5\ 10^{-3}$ m). Some samples were exposed to air as references in order to spot any eventual oxidation of the compound. The diffusion spectra, scattered by the samples irradiated with graphite-monochromatized silver K_α (0.560 83 Å) radiation, were obtained using a home-built dedicated diffractometer. All data sets included 580 measurements collected at room temperature in the range $0° < \theta < 65°$ for equidistant s values ($s = 4\pi\ (\sin\theta/\lambda)$; $\Delta s = 0.035\ Å^{-1}$). Diffusion spectra from air and from a capillary filled with pure PVP powder were also collected in the same conditions. The raw intensity scattered by the sample was corrected for air, capillary, and PVP contributions in order to extract scattering from the particles only (assuming weak interactions between cobalt and PVP). Polarization and absorption corrections were also applied. Data were normalized according to Norman and Krogh-Moes method.[17] A structure-related component, the so-called reduced intensity $i(s)$, and its Fourier transform, the reduced radial distribution function (RDF) that shows the distribution of interatomic distances in the sample, were calculated as given in Ref. 18.

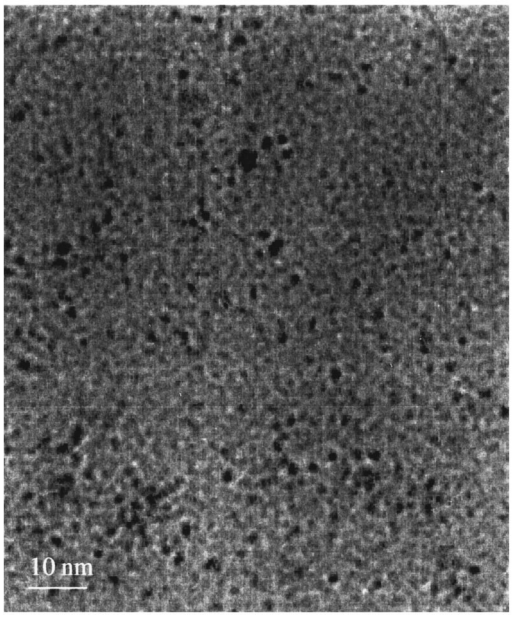

FIG. 1. Low magnification TEM micrograph of small Co particles in Coll-I.

Magnetic studies were carried out on dried colloid sample prepared in an argon dry box to prevent any uncontrolled oxidation. Low-field susceptibility and magnetization up to 5.5 T were made using a MPMS 5.5 Quantum Design superconducting quantum interference device (SQUID) Magnetometer where the temperature could be varied from 2 to 400 K. High-field magnetization up to 35 T was carried out by using the facilities of the S.N.C.M.P. in Toulouse (France).[19] The pulsed field increases according to a sinus law and reaches its maximum in a time of 0.1 s, and decreases according to an exponential law in 1.6 s. These measurements were scaled upon those performed in the SQUID for $B = 5$ T.

III. RESULTS

A. Particle morphology and structure

The size distribution of the samples was measured from low magnification micrographs as the one presented in Fig. 1. To enhance the nanoparticles TEM contrast, the low magnification micrographs were highly underfocussed in order to get Fresnel fringes surrounding the grains. Such images evi-

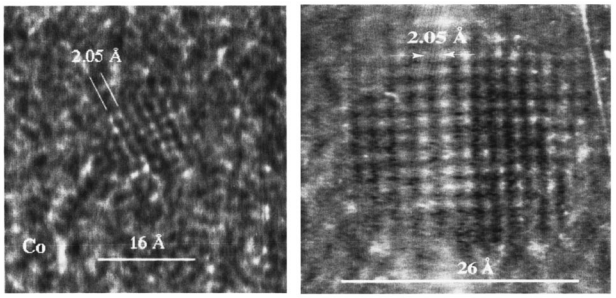

FIG. 2. HRTEM micrograph of two Co particles (diameter: 16 and 26 Å in Coll-I revealing bcc crystalline structure.

dence the presence of nonagglomerated small particles homogeneously dispersed in the polymer. Numerical image analyses were performed after digitizing the images and size histograms were calculated.[20] They reveal a narrow diameter distribution centered around 1.5 and 2 nm for Coll-I and Coll-II, respectively. However, because of the Fresnel fringes, it may be either overestimated or underestimated by a few angstroms (about 2 Å). HRTEM experiments were then used to determine the fine structure of the particles. HRTEM lattice images were digitized and the interplanar angles and spacings were measured from the corresponding numerical diffractograms (Fourier transforms). Direct interpretation of the structural feature in term of projected potential is favored when the particles are observed along suitable directions. For instance, a HRTEM micrograph of fcc particles can be directly interpreted when they are observed with their [110]- (respectively, [001]-) type directions parallel to the electron beam. In these directions of observation, the lattice images reveal the three $(1\bar{1}1)$, $(11\bar{1})$, and (002) set of planes [respectively, the two (200) and (020) planes] with angles between them of 70.5° and 54.7° (respectively, 90°). Bcc particles will be easily recognizable when observed along their [001]-type directions (respectively, [111]) that permits the observation of the (110) and $(1\bar{1}0)$ perpendicular planes [respectively, the three $(0\bar{1}1)$, (101) and $(1\bar{1}0)$ planes making 60° angles between them].

HRTEM experiments generaly reveal nonperfect lattices due either to nonoriented and/or highly distorted particles. In some cases, perfect lattices were imaged but evidence for neither Co-fcc nor Co-hcp structures is observed. Moreover, when particles were studied along a suitable direction, they usually exhibit a square lattice with interplanar distances of about 2.05 Å (± 0.05). Two HRTEM micrographs of particles of different sizes (16 and 26 Å) exhibiting such square lattice are reported in Fig. 2. Such a square lattice image cannot be due to a Co-fcc particle, since in this case the lattice image would be formed by two (002) perpendicular planes whose spacing of 1.77 Å does not correspond to that which is measured. Moreover, this lattice distance is less than the point resolution of the microscope and therefore cannot be imaged. Such a square lattice could originate from Co-bcc particles observed along the [001] direction that exhibit two perpendicular (110)-type planes. In this hypothesis, the parameter of the Co-bcc cell would be 2.9 Å (± 0.05). Such a square lattice contrasts could also be due to CoO-fcc particles ($a = 4.26$ Å) observed along their [001]-type directions that show the two (200) and (020) perpendicular planes with interplanar distances of 2.13 Å. HRTEM experiments were then performed making focus series and comparing them with simulated images of both the Co-bcc and CoO-fcc cells. These simulations do not show sufficient contrast difference between the Co-bcc and the CoO-fcc models and so do not permit rejection of either of the two models. However, since the samples for TEM were carefully prepared in the absense of oxygen, and since no oxides were observed either in WAXS experiments or in magnetic measurements (see the following sections), the presence of the oxide in the sample was rejected. Moreover, if CoO-fcc particles were present in the preparation, they also should appear with much higher contrast in HRTEM images when observed along the [110]-type directions ($d_{(111)}$CoO-fcc$= 2.45$ Å).

Consistent sets of data were obtained from WAXS measurements of different samples. Several patterns have been obtained for samples prepared under argon and samples exposed to air. Because of the very distinct patterns produced by the protected particles compared to the exposed ones, it may be assumed that no or negligible oxidation took place in the original sample.

Direct analysis of the experimental function only allows an approximate measurement of the metal-metal bond length and of the extent of the order inside the sample because of the complexity of the RDF produced by the large number of atoms included in particles of nanometric size. In order to further investigate the structure, a model must be defined. From this model, the theoretical functions for intensity and radial distribution can be computed using the Debye's formula.[21] The theoretical functions can then be checked and refined against the experimental ones. Here, we applied an approach previously described[18] that is based on the characteristic distance distributions exhibited by the different kinds of packing. In order to determine the crystalline structure, hcp and fcc structures have been considered. However a bcc structure has also been considered, since it was proposed on our particles in HRTEM experiments.

An hcp model was built from the structure of bulk cobalt at room temperature. fcc and bcc models were also built from reference lattices, the cell parameter being adjusted in order to set the shortest cobalt-cobalt distance to 2.50 Å as in the bulk. All models were built to be spherical in shape with a diameter of approximately 14 Å for Coll-I, according to the results from magnetic studies and HRTEM observations. However, well-defined structural features vanish above 9 Å in the RDF (Fig. 3) that might indicate poorly organized layers close to the surface of the particles. A global disagreement between experimental and simulated patterns allows us to discard the fcc model. bcc and hcp give more ambiguous elements (Figs. 3 and 4). Allowing for an adjustment of the shortest metal-metal distance from 2.50 Å down to 2.43 Å, for the bcc structure both models generate peak pattern for distances consistent with those observed. However strong discrepancies remain. The RDF computed from a 137 atoms bcc model exhibits strong discrete peaks which cannot be observed in experiment. The first peak is also asymmetrically broadened. This results from a contribution of the second interatomic distance significantly larger than the first one in the bcc structure (a vs $a\sqrt{3}/2$). This distance does not fit the sharper profile in the experimental function. The RDF computed from a 156 atoms hcp model does not show these two

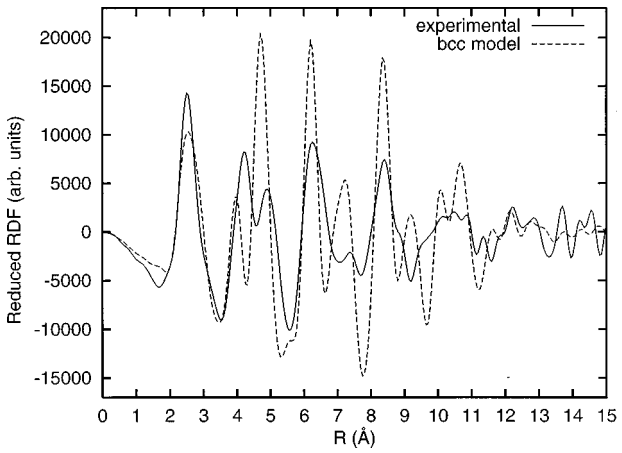

FIG. 3. Experimental (solid line) and simulated (dashed line) reduced RDF: (bcc model) (Coll-I).

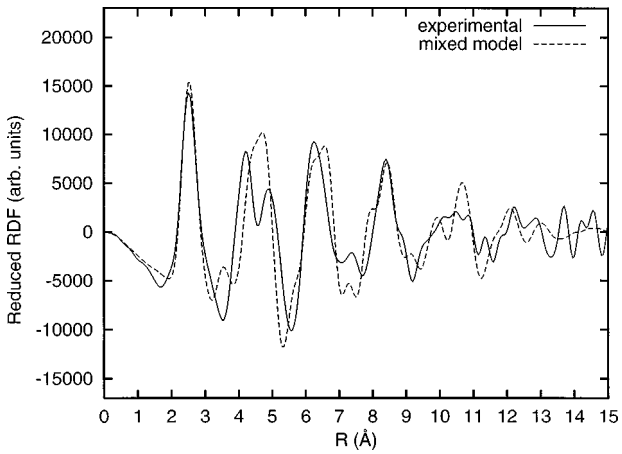

FIG. 5. Experimental (solid line) and simulated (dashed line) reduced RDF: (mixed structure model) (Coll-I).

defects, but because of extra peaks, especially at 3.6 and 7.9 Å, a purely hcp model is also not suitable. We, however, observed a strong correlation between the locations for maxima and minima introduced by bcc and hcp models, both in real and reciprocal space. We also investigated a mixed model including particles of both structures. We actually observed a much better global agreement for a model including 30% of bcc particles and 70% of hcp ones, even if still far from perfect (Fig. 5).

Since no hcp particles were observed by HRTEM, these results might indicate that local order for cobalt in these very small particles is not the same for the core and the surface. In this hypothesis, the atoms closest to the center should adopt the observed bcc structure with a short metal-metal bond length, whilst at the surface a more relaxed organization should introduce a distribution of distances close to those of an hcp structure. As is shown in Fig. 2, the HRTEM micrographs reveal several defects in the atomic periodicity near the surface. Normally, metallic cobalt adopts a hcp structure or a metastable fcc structure. However bcc structure can be stabilized via epitaxial growth on GaAs substrates.[22] For the two samples, the mean parameter of the core Co-bcc cell is 2.8 Å (± 0.05) with a shortest metal-metal distance estimated to 2.43 Å (from WAXS patterns), in agreement with the one measured on the whole particle [2.9 Å (± 0.05) from HRTEM micrographs]. The lattice parameter deduced from WAXS patterns is very close to the one observed on thin bcc cobalt films.[22] However, in spite of this agreement, this result is very surprising since small particles are expected to have a fcc-like structure.[23]

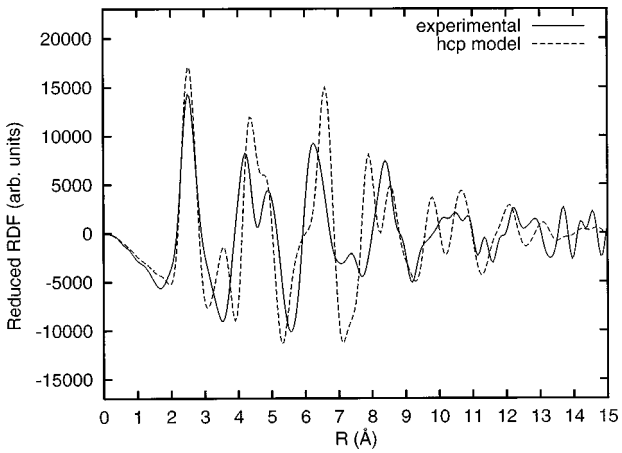

FIG. 4. Experimental (solid line) and simulated (dashed line) reduced RDF: (hcp model) (Coll-I).

B. Magnetic properties

We report hereafter the main results obtained on the magnetic properties of Coll-I and Coll-II measured in the solid state as powders. A typical temperature dependence of zero-field cooled magnetization (ZFCM) and field cooled magnetization (FCM) is shown in Fig. 6. In order to obtain these curves, the sample was cooled in zero field from room temperature to 5 K. Then, a magnetic field of 1 mT was applied and the ZFCM was measured with increasing the temperature from 5 to 400 K, after which the FCM was measured in the same applied field from 400 to 5 K with decreasing the temperature.

The ZFCM presents a narrow maximum at $T_B = 9$ K, and a large irreversibility starting at $T_D = 25$ K in the field cooled process. The inset of Fig. 6 shows inverse magnetization dependence vs temperature. For $T > T_B$, the data fall on a straight line intercepting $T_0 = 0 \pm 1$ K, according to a Curie law.

This behavior is characteristic of a superparamagnetic assembly of ferromagnetic particles (see Appendix A).[24] The low value of T_0 shows the weakness of the interparticlar interactions (see Appendix B). In order to confirm this behavior, we measured the magnetization for temperatures above the blocking temperature. As expected for superparamagnetism,[24] the data fall on a single curve (Fig. 7) when plotted vs applied field divided by temperature $[M(B/T)]$.

A more precise analysis of these measurements can be perfomed in the framework of superparamagnetism (see Appendix A). The ZFCM and FCM curves can be fitted with a log-normal size distribution

$$f(d) = \frac{1}{\sqrt{2\pi} d \sigma} \exp - \left\{ \frac{[\ln(d) - \ln(d_0)]^2}{2\sigma^2} \right\}, \qquad (1)$$

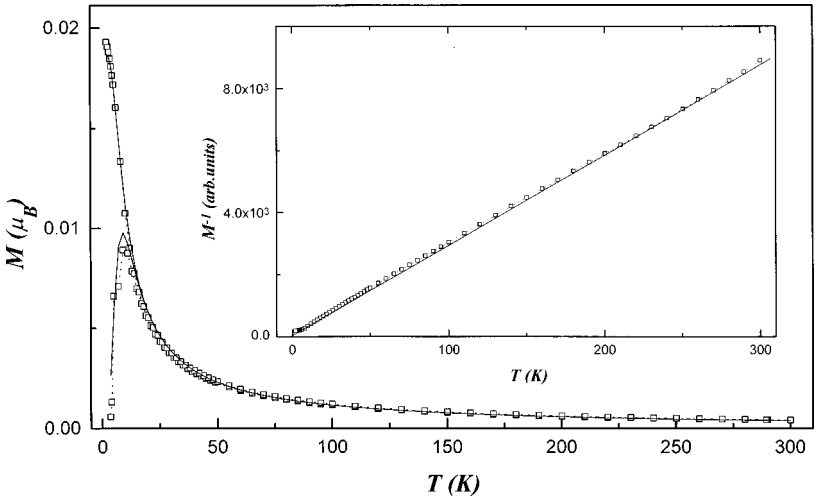

FIG. 6. ZFC and FC magnetizations vs temperature for Coll-I. Inset shows inverse ZFC and FC magnetizations vs temperature following a Curie law (symbol: experimental; dashed line: simulation).

where d_0 and σ are the mean diameter and the width of the distribution, respectively, (see Figs. 6 and 7). These investigations allowed us to determine precisely the size distribution, the effective magnetic anisotropy (K_a), and the average magnetic moment per Co atom of the particles (see Table I). We find very narrow size distributions ($\sigma<0.18$) for both samples with diameters centered around 1.5 nm for Coll-I and 1.9 nm for Coll-II (Fig. 8). As the particle size distribution is very narrow the $M(B/T)$ curves can be well fitted using a single Langevin function (see Fig. 7). We deduce the mean magnetic moment per particle, in good agreement with the parameters determined above. We thus extract the mean size with a very good accuracy, and find it to be 150 ± 10 and 310 ± 20 atoms per particle for Coll-I and for Coll-II, respectively. This allows us to confirm that the size distribution is very narrow. Moreover, since the magnetic interactions between the particles are negligible, we conclude that the particles are well separated and dispersed in the polymer. These results confirm the ones previously obtained from HRTEM and WAXS experiments.

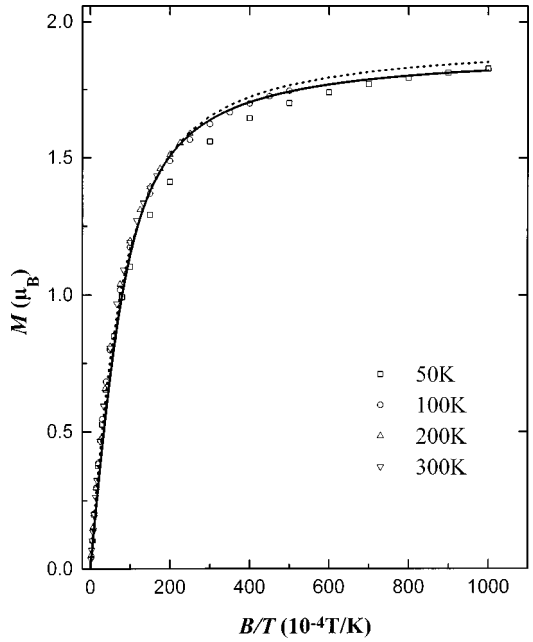

FIG. 7. Magnetization vs applied field divided by temperature for temperatures between 50 and 300 K. The dashed line and straight line present theoretical magnetization following a Langevin law with a size distribution and a simple Langevin law, respectively.

The effective magnetic anisotropy (K_a), and the mean magnetic moment per cobalt atom ($\langle\mu_{\mathrm{Co}}\rangle$), are slightly enhanced as compared to bulk fcc or hcp phases Co and increase as the particle size decreases (Table I). The coercive field has been estimated to be 0.025 T for Coll-I and 0.059 T for Coll-II at 5 K. In order to determine more precisely the values of K_a and $\langle\mu_{\mathrm{Co}}\rangle$, magnetization loops up to 5 T (insets Figs. 9 and 10) have been measured. As expected for temperatures below the blocking temperature,[24] a hysteristic behavior is observed. In order to confirm that saturation is achieved, an initial magnetization curve up to 35 T at 4.2 K is measured. It shows that the magnetization does not saturate and still increases with applied magnetic field for both samples (Figs. 9 and 10). These measurements were calibrated using the pulsed field remanence curve with those measured by SQUID. Since the rate of the decrease of the pulsed field is slow, we considered and verified that no deviation occured between the two measurents.

We analyze these results considering the law of approach to saturation of an assembly of particles with uniaxial anisotropy,[25]

$$M(B)=M_s(T)\left\{1-\frac{k_BT}{M_s(T)vB}-\frac{4}{15}\left[\frac{K_a}{M_s(T)B}\right]^2\right\}. \quad (2)$$

We tried to fit the magnetization curves up to 35 T with Eq. (2) using the mean volume deduced previously. However, even setting the volume as a free parameter, Eq. (2) is inadequate to describe the approach to saturation. The introduction of a size distribution and a contribution of isolated paramagnetic impurities is not sufficient to explain the high-field dependence observed, since both lead to saturation in magnetic fields in the range of 5 to 10 T. So it clearly appears that the origin of this effect is confined in the particles. In order to quantify the changes in the magnetization of the

TABLE I. Parameters for Coll-I and Coll-II deduced from the analysis of ZFCM, FCM, and $M(B/T)$ curves. (a) Estimated from the ZFCM and FCM, (b) estimated from the magnetization measurement for $T > T_B$ for $B = 5$ T.

Sample	T_B (K)	Diameter[a] (nm)	σ[a]	$\langle\mu_{Co}\rangle$ (μ_B)[a] (a)	(b)	K_a[a] (10^6 J/m^3)
Coll-I	9	1.5±0.1	0.18±0.02	1.65±0.1	1.94±0.05	0.83±0.1
Coll-II	13.5	1.9±0.1	0.17±0.02	1.7±0.1	1.83±0.05	0.73±0.1

[a]Estimated by fitting ZFCM, FCM, and $M(B/T)$ curves (see text).

particles, we include in Eq. (2) a variation of the magnetic moment with the applied magnetic field $M_s(B)$ allowing us to deduce the average magnetic moment per cobalt atom [$\langle\mu_{Co}(B)\rangle$]. The results are given in Table II. $\langle\mu_{Co}\rangle$ vs the applied magnetic field is plotted in Fig. 11. $\langle\mu_{Co}(B)\rangle$ presents a variation in two stages for the two samples: a rapid one in fields up to 3–4 T and a quasilinear one in fields up to 35 T. These increases are more significant for the smallest particles.

IV. DISCUSSION

The decomposition of the organometallic precursor Co(η^3-C_8H_{13})(η^4-C_8H_{12}) (Ref. 15) in the presence of a stabilizing polymer leads to the synthesis of Co particles. By changing the initial conditions, two sizes of particles have been obtained. HRTEM studies evidence particles regularly dispersed in the polymer with narrow log-normal size distribution centered around 1.5 and 2 nm (±0.2 nm) for Coll-I and Coll-II, respectively. These results have been confirmed by the analysis of ZFCM, FCM, and $M(B/T)$ in terms of superparamagnetism. Moreover, $M(B/T)$ is well fitted with a single Langevin function without taking into account the size disribution. This allows us to deduce the mean particle size with small error bars, 150±10 and 310±20 atoms for Coll-I and Coll-II, respectively.

From the magnetic studies, one can see that $\langle\mu_{Co}(B)\rangle$ increases with applied magnetic field and is enhanced (for $B > 3$ T) compared to bulk values; these features increase with decreasing mean particle size. As suggested by Fig. 11, the variation of $\langle\mu_{Co}(B)\rangle$ occurs in two stages: a rapid one in fields up to 3 T and a slow one in higher fields. Similar effects have been reported in Ref. 10 for ligated Ni and Co particles. However, in our case, we should be careful with the low-field value since its uncertainty is large. So, in the next part of the discussion, we will just focus on the high-field portion of $\langle\mu_{Co}(B)\rangle$.

The effective magnetic anisotropy (K_a) has also been found to be enhanced compared to the bulk values ($K = 4.5\ 10^5$ J/m^3 and $2.5\ 10^5$ J/m^3 for a hcp and fcc structure, respectively).[26] K_a has been determined by three methods (see Table II). K_a (c) which has been deduced from T_B via Eq. (A3) is clearly overestimated because T_B is mainly determined by the biggest particles of the size distribution. On

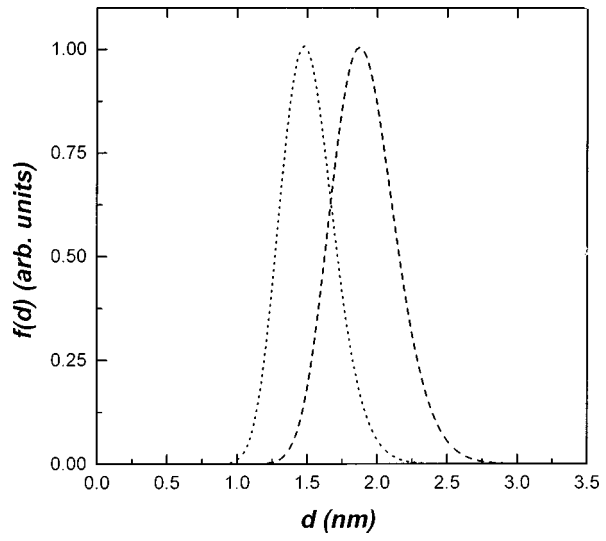

FIG. 8. Size distributions of the colloids deduced from the analysis of ZFCM, FCM, and $M(B/T)$ curves.

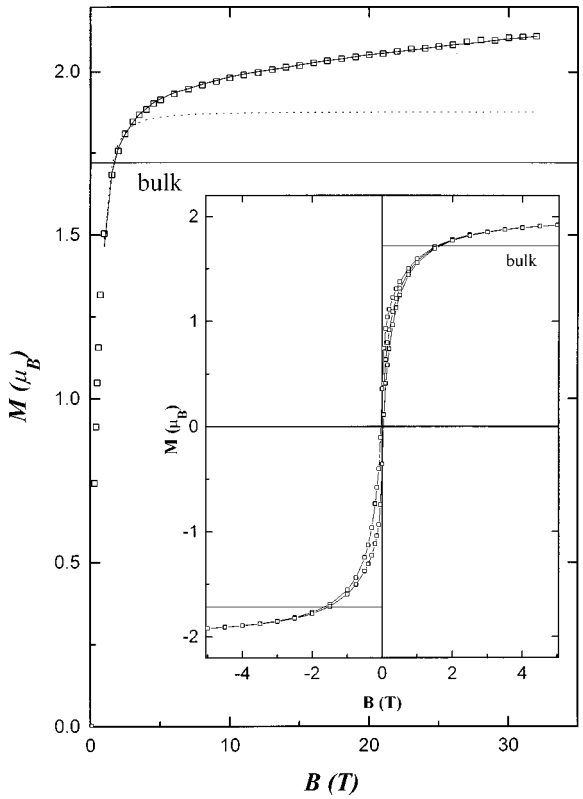

FIG. 9. Experimental initial magnetization up to 35 T for Coll-I (symbols). Inset presents the hysteresis loop at 5 K. The solid line shows the theoretical magnetization using Eq. (2) and $\langle\mu_{Co}(B)\rangle$ presented in Fig. 11. The dashed lines present theoretical magnetization curves for a constant value of $\langle\mu_{Co}(B)\rangle$. The straight line indicates the bulk value magnetic moment per Co atom.

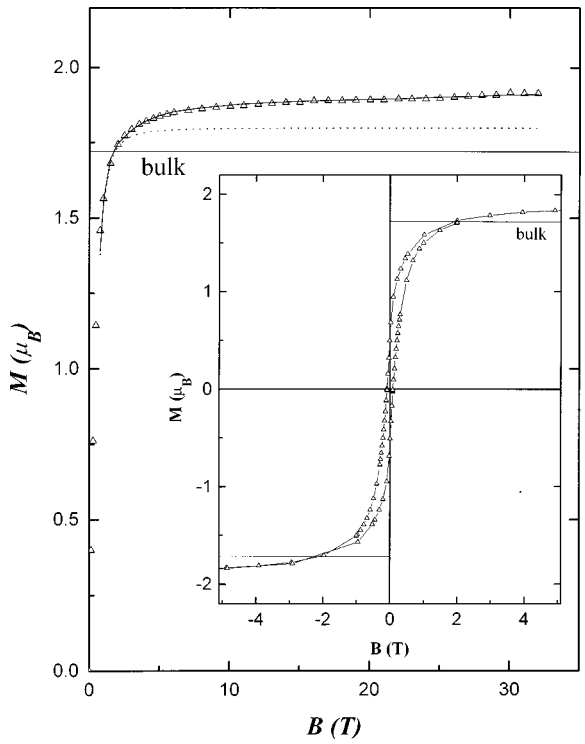

FIG. 10. Experimental initial magnetization up to 35 T for Coll-II (symbols). Inset presents the hysteresis loop at 5 K. The solid line shows the theoretical magnetization using Eq. (2) and $\langle \mu_{\mathrm{Co}}(B) \rangle$ presented in Fig. 11. The dashed lines present theoretical magnetization curves for a constant value of $\langle \mu_{\mathrm{Co}}(B) \rangle$. The straight line indicates the bulk value magnetic moment per Co atom.

the other hand, the values deduced from the fitting of ZFCM and FCM [K_a (a)], and from the approach of saturation [K_a (b)] are of the same order of magnitude and give a more reliable value. In all the cases, K_a is found to be enhanced compared to bulk value. Another way to determine K_a is the analysis of the coercive field variations vs temperature.[24] For Coll-I and Coll-II, the estimation of K_a gives a slighty lower value compared to the one deduced from the approach of saturation.[27]

Before discussing these effects, the polymer influence on the particle magnetic properties should be estimated. In order to do it, magnetic measurements on carbonyl bonded particles (Coll-I′) have been performed. They demonstrate a reduced magnetization $\langle \mu_{\mathrm{Co}} \rangle = 0.4\ \mu_B$ (at $B = 5$ T and $T = 5$ K), and the absence of blocking temperature (for $T > 5$ K) compared to Coll-I.[14] This can be interpreted in terms of a reduction of the magnetic volume, the magnetic moments of surface Co atoms bonded to carbonyl ligands being quenched. Similar quenching effects have been observed on

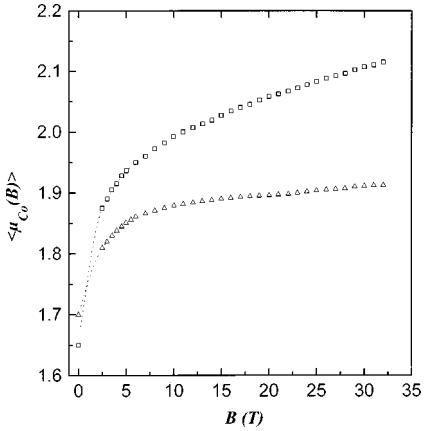

FIG. 11. Mean magnetic moment per Co atom $\langle \mu_{\mathrm{Co}} \rangle$ vs applied field. (□) for Coll-I and (△) for Coll-II. The low-field value [$\langle \mu_{\mathrm{Co}}(B = 1\ \mathrm{mT}) \rangle$] have been estimated from the ZFCM and FCM fits, while the high-field values [$\langle \mu_{\mathrm{Co}}(B) \rangle$] from the analysis of the approach to saturation. The dashed lines between low fields and high fields are guides to the eye.

Ni-carbonyl clusters[10] and attributed to a ''metallic'' magnetic character of the internal Ni atoms, while the outer are diamagnetic. These obsevations on Ni-carbonyl clusters are in agreement with theoritical predictions.[28] The addition of ligands at the surface of particles always leads to a reduced magnetization of the particles. In all the cases, we conclude to the presence of a core shell structure where the ferromagnetic core is surrounded by an antiferromagnetic, paramagnetic, or diamagnetic layer depending on the nature of the bonding at the surface. In particular, exposition to air leads to the growth of an oxide layer, which can be evidenced by shifted hysterisis loops measured after a field cooling, compared to the centered hysterisis loops measured after a zero-field cooling. The absence of such effects and moreover the enhanced magnetizations suggest that the cobalt particles do not display strong electronic interactions with the polymer and are not oxidized.[29] Since the HRTEM micrograph and the magnetic studies show that the particles are well separated and display a very narrow size distribution, we propose that through the study of an assembly of particles, we obtain some of the magnetic properties of a single one.

The mean magnetic moment per cobalt atom ($\langle \mu_{\mathrm{Co}} \rangle$) determined from the low-field experiments ($B < 5$ T) has been found to be enhanced compared to bulk value, increasing with decreasing size. Enhanced magnetic moments have been previously observed in free clusters of $3d$ metals[3,4] and on supported Co fine particles.[9] Enhanced surface magnetism has been predicted where both spin and orbital magnetic moments increase with the reduction of the coordination number.[6,7] This has been directly observed by x-ray mag-

TABLE II. Parameters for Coll-I and Coll-II. (a) Estimated by fitting ZFCM, FCM, and $M(B/T)$ curves, (b) estimated with Eq. (2), (c) estimated with Eq. (A3).

		$\langle \mu_{\mathrm{Co}} \rangle$ (μ_B)		K_a (10^6 J/m^3)		
Sample	$\langle N \rangle$ (atoms)	$B = 5$ T	$B = 30$ T	(a)	(b)	(c)
Coll-I	150±10	1.94±0.05	2.10±0.1	0.83±0.1	1.0±0.1	1.75
Coll-II	310±20	1.83±0.05	1.90±0.1	0.73±0.1	0.83±0.1	1.3

netic circular dichroism measurements on ultrathin layers.[30] Since the crystalline structure does not change drastically the value of the magnetic moment per Co atom ($\mu_{Co}=1.6-1.7$ μ_B for bcc, fcc, and hcp crystalline structures),[31] the increase of $\langle\mu_{Co}\rangle$ determined at 5 T, as the surface-volume ratio increases, clearly demonstrates the major role played by surface atoms. The mean magnetic moments per Co atom, $\langle\mu_{Co}\rangle=1.94\pm0.05$ μ_B for Coll-I and $\langle\mu_{Co}\rangle=1.83\pm0.05$ μ_B for Coll-II, are close to the one measure by Billas and co-workers[4] on free Co clusters where $\langle\mu_{Co}\rangle=1.95-2.0$ μ_B and $\langle\mu_{Co}\rangle=1.8-1.85$ μ_B for a cluster of 150 and 300 atoms, respectively. These results confirm the poor influence of the polymer on the magnetic properties. Moreover, high-field measurements show the increase of $\langle\mu_{Co}\rangle$ with applied field, leading to $\langle\mu_{Co}\rangle=2.1\pm0.1$ μ_B for coll-I at $B=35$ T, which is 25% higher than bulk value.

It is a common feature that the magnetization of fine particles does not saturate. For ferrimagnetic particles, for instance γFe_2O_3, it has been concluded that the magnetic moment within such small particles are neither parallel nor antiparallel to each other. In that case, the noncollinear spin structure was explained as a surface[32] or as a pure bulk effects.[33] The unsaturation was also observed on α-Fe in alumina[34] and Fe-O (Ref. 35) particles. This effect was attributed to the presence of an oxide shell surrounding the ferromagnetic α-Fe core[34] and to the amorphous crystalline[35] structure, respectively. In our case, since the particles are metallic and relatively ordered, we reject these hypothesis and try to connect this feature to the enhanced effective magnetic anisotropy.

Enhanced anisotropies are currently observed on fine magnetic particles and have been predicted by theoretical calculations.[36] The volume dependence of K_a can be analyzed on the basis of a simple model in which the total energy barrier is written,

$$\Delta E=K_v'v+K_s's, \tag{3}$$

where K_v' and K_s' are the volume and the surface uniaxial anisotropy energy constants, respectively, and v and s are the volume and the surface area of the particle. For spherical particles with diameter d, Eq. (3) gives

$$K_a=K_v'+\frac{a_s}{d}K_s', \tag{4}$$

where $a_s=6$. This dependence has been experimentally shown by Bodker and co-workers on α-Fe particles.[37] However, if the particles are assumed to have spherical shape, obvious symmetry arguments show that the total effective magnetic anisotropy is not affected by surface and remains the bulk one. Nevertheless, this model becomes wrong for ultrafine particles with a few number of layers. As shown by Dimitrov and Wysin, who solve numerically the Landau-Lifschitz-Gilbert equation considering a particle with classical spins in interaction through a Heisenberg exchange and an uniaxial anisotropy on surface sites, the coercive field is not zero for sufficiently small particles, and increases with decreasing particle size.[38] A hedgehoglike spin structure for small particles is predicted in zero field, and very strong magnetic fields are needed to reach a colinear spin structure. This case is not considered with the Stoner and Wohlfarth[39] model and deserves much more work. Furthermore, in any real system, as shown by the microscopy studies, a number of defects like surface facets or distorted particles, will enhance these effects.

By using Eq. (4) and K_a (b), we estimate K_v' and K_s' to 2 ± 1 10^5 J/m^3 and 0.20 ± 0.2 10^{-3} J/m^2, respectively. The resulting calculated value of K_s' is comparable to that measured on Co surfaces (typically from 0.1 to 1 10^{-3} J/m^2).[26,30,38] However, even if this simple model gives realistic parameters, the particles present several defects, as shown by the HRTEM and WAXS studies. Therefore, the factor a_s before K_s' should not be exactly six as in the spherical morphology, but should be a more complex function reflecting the particular magnetization reversal process due to the strong uniaxial anisotropy on surface atoms. These considerations allow us to conclude that the increase of $\langle\mu_{Co}(B)\rangle$ with high applied magnetic field, the latter being more important as the particle size decreases, reveals the influence of the competition between uniaxial surface anisotropy and exchange energy on the magnetization processes when the surface/volume ratio is large. At the same time, because of the incoherent rotation of the spins of the particles that leads to a more hysteristic behavior, the effective magnetic anisotropy is found to be larger in the fine particles.

V. CONCLUSIONS

We have successfully synthesized fine cobalt particles with two different very small sizes. Magnetic and microscopy studies are consistent, indicating very narrow size distributions and a regular dispersion of the particles in the polymer. WAXS and HRTEM studies reveal a surprising bcc-like crystalline structure with a distorted surface. These particles are single domain and superparamagnetic. By using a single Langevin function for temperatures above the blocking temperature, we determine precisely the mean size of the particles 150 ± 10 and 310 ± 20 atoms for Coll-I and Coll-II, respectively. The magnetic measurements allow us to determine the average magnetic moment of cobalt atoms that increased with applied field, reaching $\langle\mu_{Co}\rangle=2.1\pm0.1$ μ_B at $B=35$ T for the smallest particles, which is 25% higher than the bulk value. These results are in relative agreement with theoritical calculations and experimental results for free cobalt clusters. The effective magnetic anisotropy is enhanced compared to bulk Co. This is due to the large influence of the surface atoms which have an uniaxial magnetic anisotropy of the same order as the one measured for Co ultrathin layers. We also demonstrate the role of uniaxial anisotropy on surfaces for the magnetization process that leads to a hedgehoglike spin structure in zero field becoming colinear with large applied magnetic fields.

APPENDIX A

In a solid matrix, the relaxation of the magnetization for a single particle with an effective uniaxial anisotropy per unit volume K_a, will follow the Néel process[40,41] characterized by a relaxation time given by

$$\tau^{-1}=f_0\exp-\frac{\Delta E(B)}{k_BT}, \tag{A1}$$

where f_0 is a frequency factor usually taken to be 10^9-10^{12} Hz. ΔE is the height of the energy barrier given in the presence of an applied field B parallel to the magnetization easy axis by

$$\Delta E(B)=K_a v\left(1-\frac{B}{B_0}\right)^2 \quad \text{with} \quad B_0=\frac{2K_a}{M_s(T)}, \tag{A2}$$

where v is the volume and $M_s(T)$ the spontaneous magnetization of the particle vs temperature. For a dc experiment at the time scale $\tau_m=10-100$ sec, the blocking temperature for a particle of volume v is given by,

$$T_B(v)\approx\frac{\Delta E(B)}{30k_B}. \tag{A3}$$

For $T>T_B(v)$, the particle magnetic moment can achieve thermal equilibrium in the time of measurement, and thus, is in the superparamagnetic state. In that case, the magnetization of an assembly of identical particles will follow a Langevin function, and its susceptibility a Curie function,

$$M(B,T)=M_s(T)[\coth(x)-1/x] \quad \text{with} \quad x=\frac{M_s(T)vB}{k_BT}, \tag{A4}$$

and

$$M(B,T)=\frac{xM_s(T)}{3} \quad \text{for} \quad x\ll 1. \tag{A5}$$

For $T<T_B(v)$, the particle magnetic moment is blocked and its magnetization depends on its magnetic history. The ZFCM and the FCM are, respectively,[42]

$$M_{\mathrm{ZFC}}^{\mathrm{bl}}(B,T)=\frac{M_s^2(T)}{3K_a}B, \tag{A6}$$

$$M_{\mathrm{FC}}^{\mathrm{bl}}(B,T)=\frac{M_s^2(T)v}{3k_BT_B(v)}B\approx\frac{30M_s^2(T)}{3K_a}B$$

$$\text{with} \quad T_B(v)\approx\frac{K_av}{30k_B} \quad \text{for} \quad B\ll B_0 \quad \text{in (3)}. \tag{A7}$$

However, in any fine particle system, there is a distribution of particle sizes that gives rise to a distribution of blocking temperatures $T_B(v)$. So the ZFCM and the FCM become, respectively,

$$M_{\mathrm{ZFC}}(B,T)=\frac{M_s^2(T)B}{3k_BT}\frac{1}{\mathcal{V}}\int_0^{v_m(T)}v^2f(v)dv + \frac{M_s^2(T)B}{3K_a}\frac{1}{\mathcal{V}}\int_{v_m(T)}^{\infty}vf(v)dv, \tag{A8}$$

$$M_{\mathrm{FC}}(B,T)=\frac{M_s^2(T)B}{3k_BT}\frac{1}{\mathcal{V}}\int_0^{v_m(T)}v^2f(v)dv + \frac{30M_s^2(T)B}{3K_a}\frac{1}{\mathcal{V}}\int_{v_m(T)}^{\infty}vf(v)dv, \tag{A9}$$

where

$$\mathcal{V}=\int_0^{\infty}vf(v)dv, \tag{A10}$$

and $f(v)$ is the size (volume) distribution. The limit volume, $v_m(T)$ equal to $30\,k_BT/K_a$, is the maximum volume particle in the superparamagnetic state. The first integral represents the contribution of the superparamagnetic particles, while the second corresponds to the blocked one. The temperature variation of ZFCM gives rise to a peak at a temperature T_B, this peak arising from the increase of the fraction of the superparamagnetic particles while their magnetization decreases due to thermal fluctuations. The FCM follows ZFCM with decreasing temperature and diverges for $T<T_D$ as the biggest particles become blocked. FCM still increases with decreasing temperature and saturates as all particles are blocked.

The model presented previously included four parameters: K_a, $M_s(T)$, d_0 (mean diameter), and σ (width of the size distribution). For a better definition of the two latter parameters, we fit in the same time the magnetization curves for temperature above the blocking temperature. As expected for superparamagnetism[24] these curves fall to a single one when the magnetization is plotted vs applied magnetic field divided by temperature. In that case, $M(B/T)$ is given by

$$M(B/T)=M_s(T)\,\frac{1}{\mathcal{V}}\int_0^{\infty}vL\left[\frac{M_s(T)vB}{k_BT}\right]f(v)dv. \tag{A11}$$

Since no noticeable variation of the saturation magnetization with temperature is observed, we keep $M_s(T)$ as a constant independent of temperature in formulas (A8), (A9), and (A11). Indeed, normally $M_s(T)$ decreases with increasing temperature. So, the inverse ZFCM and FCM should deviate from the straight line representing the Curie law. As can be seen in the inset of Fig. 6, inverse ZFCM and FCM follow a Curie law up to 400 K without noticeable deviations. This allows us to say that $M_s(T)$ is practically constant for temperatures between 5 and 400 K.

APPENDIX B

In the model presented in Appendix A, the magnetic interactions between particles have been neglected. By taking into account the magnetic dipolar interactions, Chantrell and Wohlfarth demonstrate that the magnetic susceptibility follows a Curie-Weiss-like law with a critical temperature T_0 determined by a microscopic approach.[43] The value of T_0 is obtained from the formula

$$T_0=\frac{\pi^2M_s^2D^3}{72K_B}(4\varepsilon)^{2/3}\left(1+\frac{2\delta}{D}\right)^{-1}, \tag{B1}$$

where each particle of diameter D fills a volume having a radius R, δ is the thickness of the layer of protective surfactant, and ε is the volumetric particle packing fraction. In our case with $\varepsilon=0.01$, $\delta=2D$, $D=1.6$ nm, we find $T_0\approx 2$ K for

Coll-I. Another approach developed by Dormann and Fiorani gives values for T_0 in the same order.[44] As shown in the inset of Fig. 6, inverse ZFCM above T_B presents practically a Curie law dependence ($|T_0|<1$ K), where T_0 can be neglected. Moreover, sample shape effects on T_0 as Dormann and Fiorani describe[44] have not been observed. This absence of interactions confirms the regular dispersion of the particle in the polymer as observed by HRTEM.

[1] *Clusters and Colloids, From theory to applications*, edited by G. Schmid (V.C.H., Weinheim, 1994).

[2] K. A. Easom, K. J. Klabunde, C. M. Sorensen, and G. C. Hadjipanayis, Polyhedron **13**, 1197 (1995).

[3] J. P. Bucher, D. C. Douglass, and L. A. Bloomfield, Phys. Rev. Lett. **66**, 3052 (1991); S. E. Ampsel, J. W. Emmert, J. Deng, and L. A. Bloomfield, *ibid.* **76**, 1441 (1996).

[4] I. M. L. Billas, A. Chatelain, and W. A. de Heer, Science **265**, 1682 (1994).

[5] A. J. Cox, J. G. Louberdack, S. E. Apsel, and L. A. Bloomfield, Phys. Rev. B **49**, 12 295 (1994).

[6] Zhi-qiang Li and Bing-lin Gu, Phys. Rev. B **47**, 13 611 (1993); Deng Kaiming, Yang Jinlong, Xiao Chuanyun, and Wang Kelin, *ibid.* **54**, 2191 (1996).

[7] Feng Liu, M. R. Press, S. N. Khanna, and P. Jena, Phys. Rev. B **39**, 6914 (1989); O. Eriksson, A. M. Boring, R. C. Albers, G. W. Fernando, and B. R. Cooper, *ibid.* **45**, 1868 (1992).

[8] For some leading references, see C. Petit and M. P. Pileni, J. Magn. Magn. Mater. **166**, 82 (1997); S. Gangopadhyay, G. C. Hadjipanayis, B. Dale, C. M. Sorensen, K. J. Klabunde, V. Papaefthymiou, and A. Kostikas, *ibid.* **45**, 9778 (1992); J. Rivas, R. D. Sanchez, A. Fondado, C. Izco, A. J. Garcia-Bastida, J. Garcia-Otero, J. Mira, D. Baldomir, A. Gonzalez, I. Lado, M. A. Lopez Quintela, and S. B. Oseroff, J. Appl. Phys. **76**, 6564 (1994); C. P. Gibson and K. J. Putzer, Science **267**, 1338 (1995); L. Yiping, G. C. Hadjipanayis, C. M. Sorensen, and K. J. Klabunde, J. Appl. Phys. **67**, 4502 (1990); J. A. Becker, R. Schafer, R. Festag, W. Ruland, J. H. Wendorff, J. Pebler, S. A. Quaiser, W. Helbig, and M. T. Reetz, J. Chem. Phys. **103**, 2520 (1995); V. Dupuis, J. Perez, J. Tuaillon, V. Paillard, P. Melinon, A. Perez, B. Barbara, L. Thomas, S. Fayeulle, and J. M. Gay, J. Appl. Phys. **76**, 6676 (1994).

[9] J. P. Chen, C. M. Sorensen, K. J. Klabunde, and G. C. Hadjipanayis, J. Appl. Phys. **76**, 6316 (1994).

[10] L. J. de Jongh, Physica B **155**, 289 (1989); David A. van Leeuwen, J. M. Van Ruitenbeek, L. J. de Jongh, A. Ceriotti, G. Pacchioni, O. D. Harberlen, and N. Rosch, Phys. Rev. Lett. **73**, 1432 (1994).

[11] R. Sessoli, H. L. Tsai, A. R. Schake, S. Wang, J. B. Vincent, K. Folting, D. Gatteschi, G. Christou, and D. N. Hendricsen, J. Am. Chem. Soc. **115**, 1804 (1993).

[12] L. Thomas, F. Lionti, R. Ballou, D. Gatteschi, R. Sessoli, and B. Barbara, Nature (London) **383**, 145 (1996).

[13] A. Duteil, R. Queau, B. Chaudret, R. Mazel, C. Roucau, and J. S. Bradley, Chem. Mater. **5**, 341 (1993); D. de Caro, H. Wally, C. Amiens, and B. Chaudret, J. Chem. Soc. Chem. Commun. 1891 (1994); C. Amiens, D. de Caro, B. Chaudret, J. S. Bradley, R. Mazel, and C. Roucau, J. Am. Chem. Soc. **115**, 11 638 (1993); D. de Caro, V. Agelou, A. Duteil, B. Chaudret, R. Mazel, C. Roucau, and J. S. Bradley, New J. Chem. **19**, 1265 (1995).

[14] J. Osuna, D. de Caro, C. Amiens, B. Chaudret, E. Snoeck, M. Respaud, J. M. Broto, and A. R. Fert, J. Phys. Chem. **135**, 14 571 (1996).

[15] S. Otsuka and M. Rossi, J. Chem. Soc. A, 2630 (1968).

[16] T. T. Nguyen and N. Sheppard, in *Advances in Infrared and Raman Spectroscopy*, edited by R. J. Clarke and R. E. Hester (Heyden, London, 1968), Chap. 2.

[17] N. Norman, Acta Crystallogr. **10**, 370 (1957); J. Krogh-Moe, *ibid.* **9**, 951 (1956).

[18] A. Rodriguez, C. Amiens, B. Chaudret, M. J. Casanove, P. Lecante, and J. S. Bradley, Chem. Mater. **8**, 1978 (1996).

[19] J. P. Lascaray, M. Nawrocki, J. M. Broto, H. Rakoto, and M. Demianiuk, Solid State Commun. **61**, 401 (1987).

[20] M. J. Cazanove, P. Lecante, E. Snoeck, A. Mosset, and C. Roucau, J. Phys. III **7**, 505 (1997).

[21] P. Debye, Ann. Phys. (Leipzig) **46**, 809 (1915).

[22] G. A. Prinz, Phys. Rev. Lett. **54**, 1051 (1985); P. C. Riedi, T. Dumelow, M. Rubinstein, G. A. Prinz, and S. B. Qadri, Phys. Rev. B **36**, 4595 (1987); Y. U. Idzerda, W. T. Elam, B. T. Jonker, and G. A. Prinz, Phys. Rev. Lett. **62**, 2480 (1989).

[23] D. Tomanek, S. Mukherjee, and K. H. Bennemann, Phys. Rev. B **28**, 665 (1983).

[24] C. P. Bean and J. D. Livingston, J. Appl. Phys. **30**, 120S (1959).

[25] N. Akulov, Z. Phys. **67**, 194 (1931); R. Gans, Ann. Phys. (Leipzig) **15**, 28 (1932).

[26] A. Herpin, *Theorie du Magnetisme* (Presse Universitaire de France, Paris, 1968).

[27] M. Respaud, Ph.D. thesis, Toulouse, France, 1997.

[28] N. Rosch, L. Ackermann, G. Pacchioni, and B. I. Dunlap, J. Chem. Phys. **95**, 7004 (1991).

[29] M. Respaud, J. M. Broto, L. Thomas, B. Barbara, M. Verelst, P. Lecante, E. Snoeck, T. Ould Ely, C. Amiens, and B. Chaudret (unpublished).

[30] D. Weller, J. Stohr, R. Nakajima, A. Carl, M. G. Samant, C. Chappert, R. Megy, P. Beauvillain, P. Veillet, and G. A. Held, Phys. Rev. Lett. **75**, 3752 (1995).

[31] V. L. Moruzzi, P. M. Marcus, K. Schwarz, and P. Mohn, Phys. Rev. B **34**, 1784 (1986); J. Magn. Magn. Mater. **54-57**, 955 (1986); B. I. Min, T. Oguchi, and A. J. Freeman, Phys. Rev. B **33**, 7852 (1986); D. Bagayoko, A. Ziegler, and A. Callaway, *ibid.* **27**, 7046 (1983); K. Schwarz, P. Mohn, P. Blaha, and J. Kubler, J. Phys. F **14**, 2659 (1984); F. Herman, P. Lambin, and O. Jepsen, Phys. Rev. B **31**, 4394 (1985); D. J. Singh, *ibid.* **45**, 2258 (1992).

[32] A. H. Morrish and K. Haneda, J. Magn. Magn. Mater. **35**, 105 (1983).

[33] Q. A. Pankhurst and R. J. Pollard, Phys. Rev. Lett. **67**, 248 (1991).

[34] C. Johansson, M. Hanson, M. S. Pedersen, and S. Morup, J. Magn. Magn. Mater. **134**, 25 (1994).

[35] C. Djega-Mariadassou, J. L. Dormann, M. Nogues, G. Villers, and S. Sayoui, IEEE Trans. Magn. **26**, 1819 (1990).

[36] G. M. Pastor, J. Dorantes-Davila, S. Pick, and H. Dreysse, Phys. Rev. Lett. **75**, 326 (1995).

[37] F. Bodker, S. Morup, and S. Linderoth, Phys. Rev. Lett. **72**, 282 (1994).

[38] D. A. Dimitrov and G. M. Wysin, Phys. Rev. B **50**, 3077 (1994); **51**, 11 947 (1995).
[39] E. C. Stoner and E. P. Wohlfarth, Proc. R. Soc. London, Ser. A **240**, 599 (1948).
[40] L. Néel, C. R. Hebd. Seances Acad. Sci. **228**, 664 (1949).
[41] W. F. Brown, Phys. Rev. **130**, 1677 (1963).
[42] E. P. Wohlfarth, Phys. Lett. **85A**, 489 (1979).
[43] R. W. Chantrell and E. P. Wohlfarth, J. Magn. Magn. Mater. **40**, 1 (1983).
[44] J. L. Dormann and D. Fiorani, J. Magn. Magn. Mater. **140-144**, 415 (1995).